IEEE Access
Multidisciplinary | Rapid Review | Open Access Journal

Received 9 July 2024, accepted 24 July 2024, date of publication 29 July 2024, date of current version 9 August 2024.

*Digital Object Identifier 10.1109/ACCESS.2024.3435463*

SURVEY

# An Overview of 800 V Passenger Electric Vehicle Onboard Chargers: Challenges, Topologies, and Control

**SUKANYA DUTTA, (Member, IEEE), AND JENNIFER BAUMAN, (Senior Member, IEEE)**
Department of Electrical and Computer Engineering, McMaster University, Hamilton, ON L8S 4L8, Canada

Corresponding author: Jennifer Bauman (jennifer.bauman@mcmaster.ca)

**ABSTRACT** Ultrafast charging can help increase the adoption of battery electric vehicles (BEVs) as it solves the prime issues of range anxiety and long charging time. However, for conventional 400 V battery systems, these high charging currents can become infeasible due to cable limitations and thermal issues. Fortunately, 800 V systems can provide higher charging power capacity at lower current levels, better enabling ultrafast charging. The emerging shift to 800 V systems from 400 V systems requires careful design considerations for the on-board charger (OBC). This article fills a gap in the literature by performing a comprehensive review of state-of-the-art 800 V passenger BEV OBC topologies and control, focusing primarily on 1-phase topologies as the majority of residential charging connections are 1-phase. This article also reviews the main design challenges for 800 V OBCs and relevant industrial products, and provides a discussion of related future trends.

**INDEX TERMS** AC-DC power converters, battery chargers, DC-DC power converters, electric vehicles.

## I. INTRODUCTION

The restrictions on carbon dioxide ($CO_2$) emissions due to rising environmental concerns are stimulating automotive manufacturers to reduce their $CO_2$ emissions. Battery electric vehicles (BEVs) are excellent alternatives to internal combustion engine vehicles due to their high efficiency, zero tailpipe emissions, and reduced reliance on fossil fuels [1], [2], [3]. In recent years, the global market for electrified vehicles has grown. In 2023, global sales of BEVS and plug-in hybrid electric vehicles (PHEVs) were 13.6 million, a 31% increase from 2022 [4]. Furthermore, analysis from [5] predicts the global fleet of BEVs and PHEVs will be 120 million by 2030.

However, there are still some practical challenges impeding increased BEV adoption, such as cost, long charging times, and limited driving ranges [6]. Recently, 800 V BEVs have been introduced into the market to allow higher power fast-charging, which reduces charge times while on the go, and thus can help to alleviate driver range concerns if they can rely on quick re-charging during long-distance driving days. For example, a BEV with a 60 kWh battery takes about 72 minutes to charge at the typical 50 kW fast charger, but by increasing the fast-charging power level to 150 kW, the charging time is reduced by two-thirds, down to 24 minutes. However, for a typical 400 V BEV, the charging current would also triple at this power level, leading to large conduction losses and thermal issues in the charging cables [7]. By doubling the battery nominal voltage to around 800 V, charging currents are halved, opening up opportunities for much higher charging levels [8]. An additional advantage of 800 V BEVs is that on-board wiring sizes can be reduced, decreasing wiring cost and mass [7].

Heavy-duty vehicles such as electric buses and trucks have high operating power and thus can benefit from 800 V batteries, but recently, commercial passenger vehicles have also shifted towards 800 V battery systems due to these ultrafast-charging opportunities. Porsche has introduced an 800 V nominal battery in the Taycan, allowing charging rates up to 350 kW [9], [10]. Other 800 V examples include the Aston Martin Rapide Type E [11], the Hyundai Ioniq 5 [12], the Genesis G80 EV [13], and the Audi e-Tron GT RS [14]. The Kia EV6 Wind uses a moderately high-voltage battery

The associate editor coordinating the review of this manuscript and approving it for publication was Zhilei Yao.

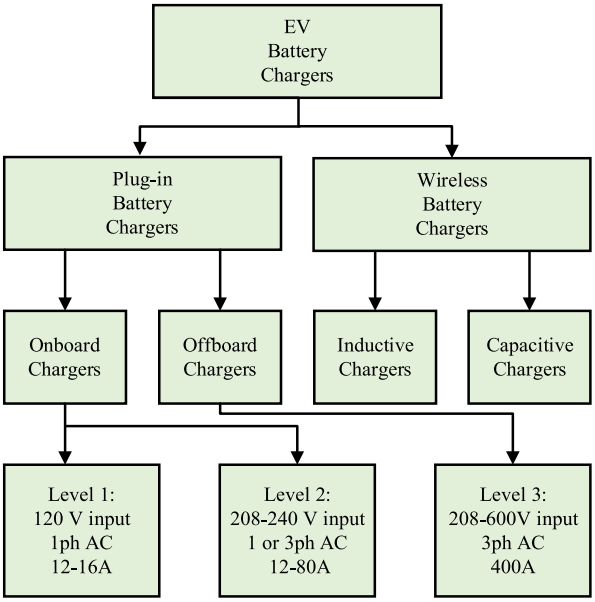


**FIGURE 1.** Overview of battery charging types and levels.

with a nominal voltage around 700 V to achieve similar fast-charging benefits [15]. To serve these new 800 V vehicles, high-voltage fast chargers have also appeared on the market, such as ABB's *Terra Hp* modular charging system, which can charge both 400 V and 800 V batteries with charging powers of 175 or 350 kW, respectively [16].

Though fast-charging is useful on long-distance driving days, many drivers will still rely on convenient low-power at-home overnight charging for most of their regular commuting days. This is advantageous for the grid because it generally has excess capacity at night [17], advantageous for the vehicle's battery lifetime because it can be shortened by excessive fast-charging events [18], and advantageous for the environment as the grid often has a lower carbon intensity overnight compared to peak load hours of the day [19].

Fig. 1 summarizes the different charging types and levels for electric vehicles. The input voltage and current for the three charging levels (1, 2, and 3) are shown where all three charging levels are capable of 800 V battery charging. This review paper focuses on 1-phase on-board chargers (Level 1 and Level 2 charging) for 800 V passenger vehicles, because the majority of residential locations have 1-phase power connections [20], and it can be quite costly to upgrade residential electrical systems to 3-phase power [21]. Though 3-phase on-board charging can provide a faster charge than 1-phase, most residential locations have 1-phase power connections and 1-phase on-board charging can provide adequate overnight charge for the majority of drivers [22]. Thus, for widespread 800 V BEV adoption primarily using cost-effective, convenient, and lower-emission overnight charging, the on-board charger (OBC) is a crucial component.

The main challenges for developing a 1-phase OBC for 800 V BEVs are: (i) a very high voltage step-up is required from 120 or 240 1-phase AC voltage to over 800 V DC, (ii) doubling the number of battery cells in series to obtain a nominal 800 V pack as opposed to a nominal 400 V pack will also double the voltage swing of the pack from low to high states-of-charge (SOC) [23], and it is more difficult to achieve high efficiency over a wider output voltage range, especially when the input voltage range may also vary with a 120 V or 240 V grid connection, and (iii) higher voltage devices may be required, increasing the on-resistance and the overall OBC cost. This review paper is the first to provide a detailed review and comparison of topologies and techniques suggested in the literature to address these challenges. Other review papers related to 800 V BEVs include [24], which provides an overview of 800 V BEVs including charging time benefits, packaging improvement, and battery structure development, [25], which provides a comprehensive analysis of how all major powertrain components will change in an 800 V BEV compared to a 400 V BEV, and [26], which provides an overview of 800 V BEV charging, including charging infrastructure and regulatory standards, where the OBC discussion focuses on 3-phase charger topologies. Furthermore, [27], [28], [29] review OBCs in general, but do not focus on the 800 V challenges. Thus, the main contribution of this paper is the review and comparison of 800 V OBCs from academia and industry, with a focus on 1-phase OBCs, which are critical since the majority of residential charging locations are wired with 1-phase power. This paper also briefly reviews 3-phase 800 V OBCs from the literature and industry to ensure a comprehensive overall review. The remainder of this article is organized as follows: Section II provides an overview of 800 V OBCs, and Section III provides a comprehensive review of state-of-the-art 800 V OBC topologies and control, including industrial OBCs. Section IV compares the different OBCs topologies from the literature and industry, and Section V-B discusses future trends. Section V-C concludes the paper.

## II. OVERVIEW OF 800 V OBCs

BEVs are usually equipped with two charging outlets: one for standard (OBC) Level 1 and Level 2 charging with a low current connection, and another for fast (offboard) Level 3 DC charging with a high current connection [30], [31], [32]. The typical two-stage OBC has a front-end power factor correction (PFC) part with a DC link capacitor and a back-end isolated DC/DC conversion part, powered from a 120 V or 240 V AC residential outlet [33], [34]. However, recent research has also proposed several single-stage topologies without the DC link [34], [35], [36] where an AC/DC converter with suitable design and modulation can provide the front-end PFC as well as the appropriate DC output voltage. In either case, the battery and AC grid are usually isolated to avoid the common mode leakage current [37]. Common choices for the isolated DC/DC converter are the LLC converter with full bridge rectifier (with soft switching capability over a wide voltage range) and the phase-shifted

**TABLE 1. Industrial 800V EV onboard chargers.**

| Model | Output Voltage (V) | Power (kW) | Typical Charging Time | Charging Level | Input Voltage (V) | Type |
|---|---|---|---|---|---|---|
| Porsche Taycan [10] | 800 | 7.2 | 9.5-10.5 hrs | 1, 2 | 120, 240 | 1 phase |
| Aston Martin Rapide E [11] | 800 | 3.6 | 3-3.5 hrs | 1, 2 | 120, 240 | 1 phase |
| Hyundai Ioniq 5 [12] | 800 | 7.4, 22 | 20-26 hrs, 3-4 hrs | 1, 2 | 120-480 | 1 phase / 3 phase |
| Genesis G80 EV [13] | 800 | 11 | 9 hrs | 1, 2 | 120, 240 | 1 phase |
| Audi e-Tron GT RS [14] | 800 | 7.4, 22 | 9 hrs 15 mins | 1, 2 | 120-480 | 1 phase / 3 phase |
| Kia EV6 Wind [15] | 697 | 10.9 | 7 hrs 10 mins | 1, 2 | 120, 240 | 1 phase |
| GaN Systems [53] | 800 | 11 | - | - | - | 1 phase |
| Infineon [54] | 250-1000 | 10 | - | - | 320-530 | 3 phase |
| Innoelectric [55] | 400-850 | 22 | - | 1, 2 | 103-440 | 1 phase / 3 phase |
| EDN-MTA [56] | 840 | 7.3, 22 | - | 1, 2 | 240-480 | 1 phase / 3 phase |
| LG-MAGNA [79] | 800 | 3.6, 7.2, 11 | - | - | - | - |
| Valeo [80] | 800 | 7, 11, 22 | - | 1,2 | 120-480 | 1 phase / 3 phase |
| Huawei [81] | 800 | 6.6, 9.9 | - | 1,2 | 120-480 | 1 phase / 3 phase |

full-bridge (PSFB) converter [38], [39]. The PFC part controls the link voltage, and the link capacitor is the primary energy storage which aids in reducing the output voltage ripple of the PFC converter [40], [41]. The OBC charger must ensure low distortion and high power factor from the current drawn from the grid in order to maximize the real power drawn from the outlet. The harmonic injection limit should follow the standard as per IEEE Std 1547-2018 [42], SAE J2894-1 [43], and IEC 61000-3-2 [44]. The PFC stage should typically maintain a THD less than 5% with near unity power factor.

Due to the move towards 800 V batteries, the OBCs need to be redesigned in order to provide a higher voltage gain to the input AC voltages and to handle a wider output voltage range. For example, a typical 800 V OBC may require a wider output voltage range such as 500-880 V [45], [46] compared to a 400 V OBC with half the number of battery cells in series, which would require an output range of 250-440 V [45], [46], [47], where the battery voltage varies within these ranges due to variations in battery SOC. The goal is to achieve high efficiency across this wide output voltage range with a varying input voltage (120 or 240 V) [48]. The wide voltage charging challenge has been somewhat explored for two-stage topologies but not much work has been done for single-stage topologies. Though OBCs are in use while parked, they do affect the official energy efficiency ratings of BEVS, since OBC efficiency is used in these calculations, so that all energy from the wall to move the vehicle is considered. Thus, it is important to achieve high efficiency across varying voltage and power ranges.

The 800 V OBC needs higher semiconductor ratings as the voltage stress is higher compared to the 400 V OBC, which can make the converter more expensive due to the increase in semiconductor cost. MOSFET and IGBT components rated at 1200 V are a good fit for these OBCs. Wide bandgap (WBG) devices, such as gallium nitride (GaN) and silicon carbide (SiC), are popular choices for OBCs due to diminished reverse recovery charge and increased electron mobility, leading to higher switching frequencies [49], [50]. Many SiC devices are rated for 1200 V but GaN devices are thus far limited to 650 V [51], [52]. Also, the higher on-state resistance of devices with higher voltage ratings can result in higher conduction losses, thus, it can be beneficial to reduce voltage and current stresses in the design of 800 V OBCs.

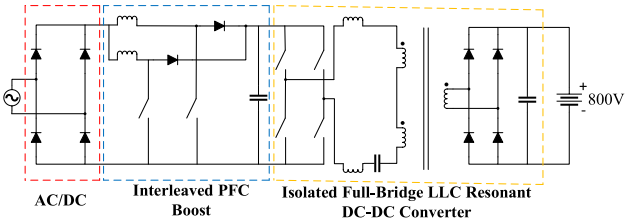


**FIGURE 2. OBC topology for GM's chevrolet volt [47].**

Table 1 summarizes the industrial 800 V OBCs, either within a vehicle (rows 1-6) or as standalone products (rows 7-13). For the six high-voltage BEVs listed, all have OBCs that can connect to 1-phase 120 V or 240 V sources. Furthermore, two vehicles, the Hyundai Ioniq and the Audi E-tron, allow on-board charging from a 3-phase connection to allow for higher power levels when needed. Infineon, Innoelectric, EDN, Valeo, and Huawei also allow 3 phase charging where Infineon has an output range from 250-1000 V and Innoelectric has an output range from 400-850 V. However, 1-phase charging is common to all high-voltage BEVS due to the widespread availability of 1-phase circuits at residential charging locations. The charging time represents the typical time required to top up the battery and it varies widely from 3 to 26 hours due to different battery sizes and different considered charging powers.

A typical two-stage 400 V OBC is shown in Fig. 2, which is used in GM's Chevrolet Volt [47]. This simple topology utilizes a single-phase diode bridge for AC/DC rectification, two interleaved boost converters for PFC and to step up the AC voltage, and an LLC converter for the isolated DC/DC conversion. Reference [47] shows a peak efficiency of 95.84% at 2.92 kW. Alternatively, Transphorm uses a well-known phase shifted full bridge topology for the DC/DC conversion part of its OBC design [39]. This topology does

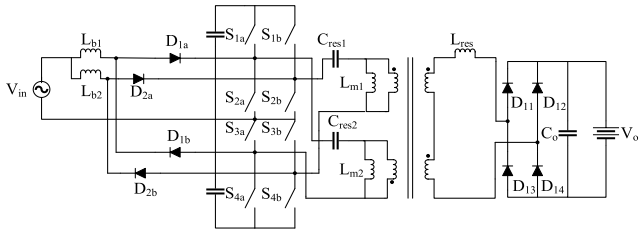


**FIGURE 3.** Interleaved bridgeless single-stage AC/DC converter with stacked switch configuration [35].

not require variable switching frequency, which is an advantage compared to LLC topologies. Transphorm GaN FETs are used for its implementation, and it achieves a peak efficiency of 97.8% at 3.3 kW. These topologies may be modified for an 800 V BEV by doubling the transformer turns ratio [25], though this will increase the transformer core size, cost, and conduction losses [57], [58]. In moving forward with 800 V OBC designs, other topologies can also be considered, with the main potential areas for enhancement being efficiency across a wide output voltage range, cost, control complexity, reliability, and power density. With this perspective, the next section reviews novel and unique topologies for 800 V OBCs, such as single-stage topologies, two-stage topologies, and integrated topologies.

## III. REVIEW OF 800 V TOPOLOGIES

### A. SINGLE-STAGE TOPOLOGIES

A single-stage isolated AC/DC interleaved bridgeless topology as shown in Fig. 3 has been proposed in [35] for 800 V BEVs considering high voltage gain and high voltage across each switch in the charger circuit. The primary intention of this converter is to enhance the overall efficiency. This converter has a modular stacked switch structure and interleaved control. The single-stage structure is created by connecting two step-up resonant circuits to the interleaved legs where the outputs are connected in series to the input of the high frequency current-fed rectifier. The high voltage gain of the charger is due to the front-end boost and the resonant circuit. The structure formed by two interleaved modules, with each module incorporating an AC/DC boost, enables all switches and diodes to have soft-switching commutation, that is, zero voltage switching (ZVS) turn-on and zero current switching (ZCS) turn-off over a wide input voltage range.

The voltage stress across each switch is half of the DC-link voltage due to the integration of the converter with CLL resonant circuits and by two legs sharing stacked switches. The switches have both the resonant current and the input inductor current flowing through them. The resonant circuit includes a resonant inductor and capacitor along with magnetizing inductance. The discontinuous conduction mode (DCM) design of the converter allows it to achieve PFC naturally. The DCM mode is achieved by keeping the average inductor current less than its current ripple. The converter has symmetrical operation and during the mode transition from switch $S_{2a}$ to $S_{1a}$, the entire switch current flows through the anti-parallel diode of $S_{1a}$. At 50% duty cycle, the peak normalized input current is achieved while operating in DCM mode. The modules 1 and 2 have the same switching frequency with a phase shift of 180°, and complimentary duty ratio control.

The converter has 27 components, including four inductors and six capacitors, one isolating transformers, eight switches rated at 650V/70A, and eight diodes rated at 1200V/18A. The 2.4 kW prototype is built using SiC MOSFETs and SiC diodes, and achieves a peak efficiency of 97.9% at 135 V. The peak efficiency for 120 V input is 97.3% at 100% load, but the efficiency drops to 93.3% at 10% load. All tests are for 800 V output, though in reality it is important to consider a wider output voltage range due to changes in the battery SOC.

This topology achieves a high peak efficiency and allows low ripple input current due to its interleaved design. However, it has lower efficiency at light load conditions for high input voltages. This circuit has a circulating current flowing through it generating conduction loss in primary switches and the transformer and the circulating current can be reduced by increasing the $L_m/L_{res}$ ratio, where $L_m$ is the magnetizing inductance and $L_{res}$ is the resonant inductance. The converter operates with duty ratio control, and the duty ratio is much lower for high input voltage range at light load condition compared to the low input voltages. Therefore, ZVS turn-on is lost in switches $S_{2a}$, $S_{3a}$, $S_{2b}$, and $S_{3b}$. The ripple reduction at the output reduces the stress on output capacitors but this increases the semiconductor count and makes the structure complex, making the control strategy complicated.

The topology in Fig. 4 has a bridgeless boost converter working in continuous conduction mode (CCM) which is integrated with an isolated CLL resonant converter along with two voltage doublers which are magnetically coupled [34]. This converter focuses on reduction of size and weight of the system. The high gain is achieved by connecting the isolated resonant inverter to the magnetically coupled high frequency active rectifiers which helps in output voltage balancing [44]. The transformer has 1:1:1 ratio incorporating leakage and magnetizing inductance in the resonant circuit. The CLL resonant converter aids the inverter as well as the active rectifier side switches to achieve soft switching. S1 and S4 achieve ZVS turn on because of the lagging resonant current (negative) flowing through these switches. These same switches achieve ZCS turn off because initially the switches are off and the voltage across them starts rising gradually. Switch S2 has zero turn on losses because at the transitioning stage the current changes from negative to positive.

This topology uses variable frequency control in order to control the output voltage and asymmetrical pulse width modulation (APWM) to accomplish PFC operation in the frontend bridgeless converter. The input current waveform is controlled using average CCM current mode control. This method results in a high-quality current waveform for varied input voltage and load power. The special feature of this

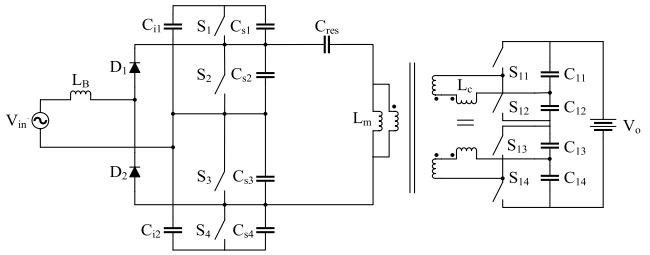


**FIGURE 4.** Bridgeless SiC-based coupled active voltage doubler rectifier [34].

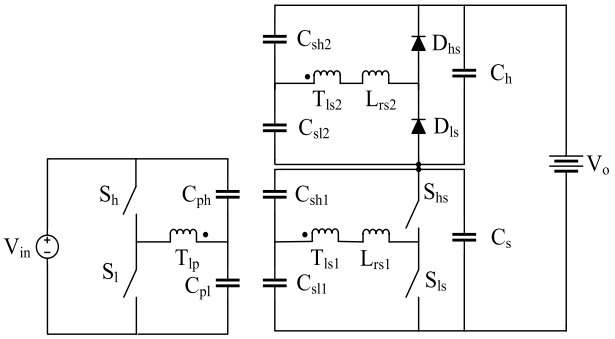


**FIGURE 5.** Tandem DC/DC converter: combination of DAB plus series resonant converter [61].

control strategy is its ability to eliminate crossover distortion [59] which are present in [60].

Due to the integrated structure, the topology has a lower component count than the topology in Fig. 3. The converter has 26 components in total, including four inductors and eleven capacitors, one isolating transformers, two diodes, and eight SiC MOSFETs rated at 650V/70A. Though simulated efficiency results are between 96% and 97% [34] for level 1 charging, experimental efficiency results are not provided. The simulated results are for 800 V output, though in reality it is important to consider a wider output voltage range due to changes in the battery SOC. Advantages of this circuit include the lack of a frontend diode bridge, reducing conduction losses, and the fact that semiconductor devices are commutated using soft switching. Furthermore, this topology does not use any complicated control scheme for balancing the output voltage in the converter modules since the active rectifiers are magnetically integrated in the output module.

The single-stage structures are proposed to reduce the additional power conversion stages and improve the overall efficiency of the converter. These structures are compact, have lower component count, and aid in improving the power density. These topologies are generally simple and cost effective. One disadvantage of single-stage structures is higher output current ripple which may result in higher output capacitor size. References [34] and [35] propose single-stage 800 V OBC designs where [35] has an interleaved design allowing lower current ripple and higher efficiency compared to [34], though [34] removes the diode bridge to enhance efficiency and has lower component count compared to [35]. Both the topologies employ resonance to accomplish soft switching. Reference [35] accomplishes PFC naturally due to its DCM design and [34] uses APWM for PFC. Overall, [35] has simpler control compared to [34].

### B. TWO-STAGE TOPOLOGIES

Two-stage topologies typically have a frontend PFC part with a DC link capacitor and backend isolated DC/DC conversion part. Thus, two-stage 800 V topologies can generally use a frontend with standard 650 V semiconductors, and the higher 800 V output is handled by the backend DC/DC converter, which may use 1200 V semiconductors. This section focuses on the backend DC/DC converter within two-stage topologies.

Reference [61] proposes a low cost and modular onboard charger DC/DC topology incorporating differential power processing [60], [62], [63] for high efficiency and power density, as shown in Fig. 5. This topology merges a dual active-bridge (DAB) [64], [65] with a series-resonant diode rectifier stage composed of diodes and the resonant tank, enabling the utilization of standard 650 V Si devices which inherently ensures optimized power processing and the appropriate output voltage distribution along with a single transformer implementation. The series resonant rectifier in this topology supplies a fixed output voltage of 450 V [61], which is the minimum battery voltage as per the design and it operates at the resonant frequency for the entire power range to ensure ZVS/ZCS operation. On the other hand, the DAB converter supplies variable output voltage as per the battery SOC. The control strategy uses phase shift modification of the DAB switches.

The converter has 17 components in total, including two inductors, eight capacitors, one isolating transformer, two diodes, and four switches rated at 650 V. The 3.6 kW prototype is built using Si MOSFETs. This topology is capable of charging both 400 V and 800 V batteries utilizing the standard 650 V super junction (SJ) MOSFET technology, improving charger cost.

Reference [2] uses a 400 V battery charger to charge an 800 V battery by dividing the battery stack into two modules which are charged alternatively by the DC/DC LLC converter using a battery selection circuit [2], as shown in Fig. 6(a). A main goal of this topology is to reduce the voltage stress on the secondary side components. This topology works in two modes: battery charging and battery changing. The operating mode is detected by sensing the battery voltages, $V_{B1}$ and $V_{B2}$. The previously optimized DC/DC converter for 400 V BEVs is switched on and off based on the selected mode. During the battery charging mode, the DC/DC converter is switched on and the switches in the battery selection circuit (BSC), $S_{A1}$ and $S_{A2}$, make a conduction path for the target battery module to be charged. The DC/DC converter is turned off while changing the battery module to be charged next as the battery voltage can affect the converter during $S_{A1}$ and $S_{A2}$ dead time. The battery module is changed after half

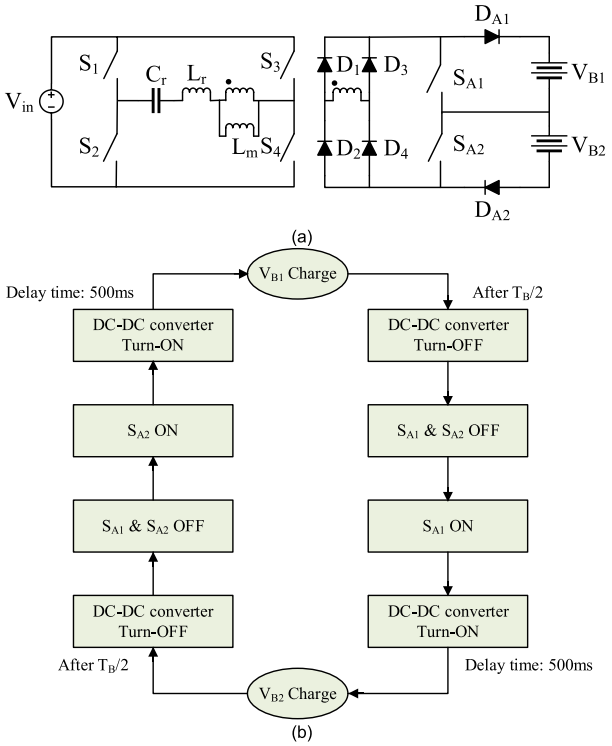


**FIGURE 6.** (a) 400V battery charger with battery selection circuit [2] (b) Battery change sequence [2].

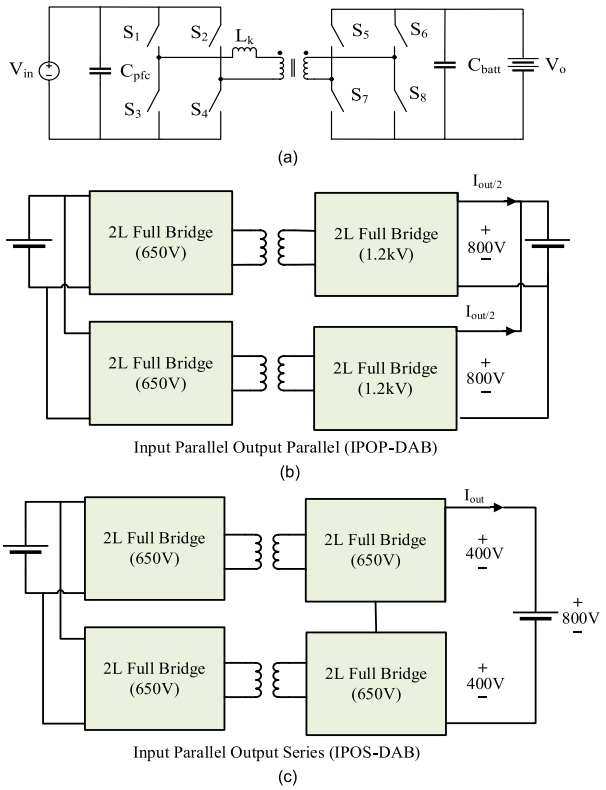


**FIGURE 7.** Dual Active Bridge and configurations derived from this converter [67].

a BSC switching cycle ($T_B/2$), and the selection switches are off during this period. The sequence of battery changing is shown in Fig. 6(b). The sum of turn-on and turn-off delay is one second.

The converter has 15 components, including one inductor, one capacitor, one isolating transformer, six switches rated at 650V/33A, and six diodes rated at 600V/45A. The 3.3 kW prototype is built using SJ MOSFETs and achieves a peak efficiency of 97.2% at 80% load. The efficiency at full load is 96.8% and the efficiency at light load is 91%. By utilizing an optimized 400 V charger with lower-rated semiconductors, cost can be reduced, but higher secondary currents will exist due to the lower secondary voltage. Also, conduction losses in the selection switches and diodes can reduce efficiency.

The DAB topology shown in Fig. 7(a) can potentially be used to improve the power density of 800 V OBCs [66], [67]. The DAB converter has a simple operating principle where two active bridges are connected through a transformer and are phase shifted from one another in order to control the amount of power flow from one DC source to the other. The topology is capable of both forward and reverse power flow. The source bridge leads the load bridge during forward power flow and the load bridge leads the source bridge during reverse operation. This converter is capable of soft switching, though the soft switching region reduces under light load condition. This configuration permits a fixed frequency operation using square wave mode and utilizes transformer leakage inductance as the primary energy transfer component.

To accommodate switching limitations, cost, hardware redundancy, and modularity, input parallel output parallel (IPOP-DAB) [67] and input parallel output series (IPOS-DAB) [67] configurations have been derived from the DAB topology shown in Fig. 7(b) and 7(c). The IPOP-DAB and IPOS-DAB have twenty-two components including four capacitors, two isolating transformers, and sixteen switches. The IPOP-DAB uses MOSFETs rated at 1200V/32A, and the IPOS-DAB uses MOSFETs rated 650V/47A. A 11.5 kW simulated model is built using SiC MOSFETs in [67], which achieves a highest average simulated efficiency of 96.12% for IPOP-DAB and 96.22% for IPOS- DAB. This topology has been simulated for 500-850 V output voltage range. The IPOP-DAB achieves the highest simulated efficiency of 96.9% at 500 V and lowest efficiency of 95.35% at 850 V whereas the IPOS-DAB achieves the highest simulated efficiency of 96.4% at 600 V and lowest efficiency of 96.18% at 712 V. The IPOP-DAB semiconductors have higher switching losses, but the conduction loss is reduced as the current flowing through these is half the rated load current. The battery side capacitor size can be reduced by interleaving. Due to its parallel operation, the IPOP-DAB offers better fault-tolerant capability compared to the IPOS-DAB.

Fig. 8(a) and (b) shows a neutral point clamped (NPC) based 2L-5L multilevel (ML) DAB topology where the bridges are assumed to have different voltage levels [67], [68]. The topology shown in Fig. 8(b) focuses on cost reduction by using lower voltage semiconductors. The three-level

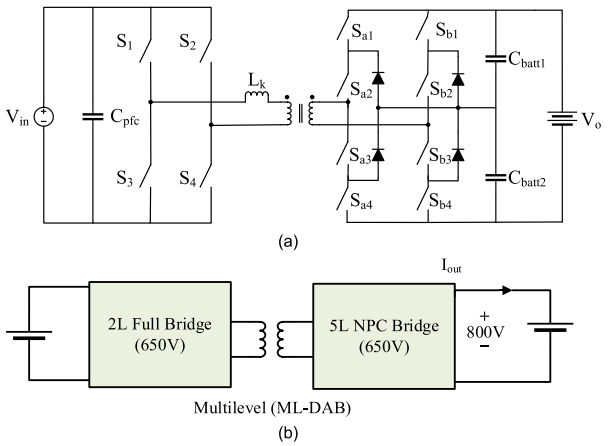


**FIGURE 8.** Multilevel DAB and configuration derived from ML DAB [67].

diode clamped legs are used to produce five-level voltage waveforms. The low voltage bridge produces two-level square waveform across the transformer by switching. The 3L NPC uses clamping diodes to connect phase output to the neutral point producing 3L voltage at each NPC leg. Though this topology allows bidirectional power flow, [67] focuses mainly on the unidirectional power flow from 2L to 5L bridge using a single-phase transformer. This topology attains ZVS in all switches and has low current stress. In the control scheme, a phase shift is introduced to produce a 5L voltage waveform across the transformer and the 2L bridge has complimentary switching with 50% duty cycle. The switching pulses and the voltage waveforms uses angular distance rather than duty cycle to synthesize 5L voltage. A zero average symmetric waveform is formed by complimentarily switching the low voltage bridge legs at a duty cycle less than 50%. A 2L voltage is formed when duty cycle is 50% and 3L voltage is formed symmetrically at the low voltage leg when the duty cycle is less than 50%.

The ML-DAB has 20 components including three capacitors, one isolating transformer, twelve MOSFETs rated at 650V/47A, and four diodes rated at 650V/16A. A 11.5 kW simulated model is created using SiC MOSFETs and Schottky diodes, which achieves a highest average efficiency of 95.66.%, and peak efficiency of 95.9% at 850 V. In this topology, if the voltage level required is higher than the DC bus voltage, then higher voltage can be achieved by cascading multiple ML-DABs which enables large scale conversion of power.

Fig. 9 shows an LCL-T isolated DC/DC converter for onboard charging with reduced capacitor RMS current stress, which focuses on efficiency improvement for 800 V charging [49]. The stacked half-bridge (SHB) architecture is used on the primary side. The transformer magnetizing inductance can be infinitely large restricting it from storing energy, resulting in a gapless transformer, thereby increasing efficiency and power voltage doubler for HV charging which results in high switch utilization. Two DC blocking capacitors are used at the source and load sides to avoid flux saturation.

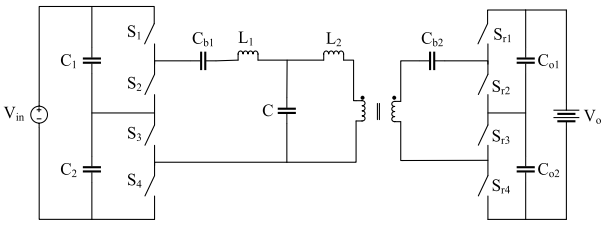


**FIGURE 9.** Stacked half–bridge (SHB) rectifier for HV battery charging [49].

The challenge to reduce output current is addressed using a modulation strategy enabling transistor soft switching along with low circulating current in constant power (CP) and constant voltage (CV) battery charging modes. The LCL-T converter output current is proportional to resonant tank input excitation. Therefore, the inverter voltage excitation can be reduced to control the output current in CP and CV charging modes. The three-level inverter is modulated by phase shifting the gate signals of S1 and S4 thereby, allowing the SHB inverter to generate the requisite output voltage.

The converter has 18 components, including two inductors, seven capacitors, one isolating transformer, and eight switches rated at 650V/60A. The 6.6 kW prototype is built using GaN transistors and achieves a peak efficiency of 97.3% at full load and 87% at light load. This converter has been tested for 330-750 V and achieves a peak efficiency of 97.6% at 580 V and lowest efficiency of 87% at 330V. The topology has the benefit of synchronous rectification, and the rectifier lags the inverter switching by a fixed time interval, which makes the synchronous rectification easier as it does not require high bandwidth current sensing. Overall, this topology achieves a competitive efficiency at wide output voltage range using 650 V semiconductor devices, and soft switching is maintained across wide output voltage and power ranges. The downside is that the control is quite complicated.

Two-stage structures have the advantage of lower current ripple and are commonly used. However, they have the disadvantage of higher power conversion stages, and lower power density. Also, the bulky DC link capacitor adds to the weight and size of the system. Reference [61] proposes the backend of a two-stage OBC which is capable of both 400 and 800 V charging. Since the topology is based on DAB and LLC, bidirectional charging and soft switching are possible. Reference [2] used a 400 V optimized OBC to charge 800 V batteries using a battery selection circuit. IPOP-DAB and IPOS-DAB proposed in [67] have highly efficient wide output voltage operating range (500-850 V). ML-DAB proposed in [67] is capable of large-scale power conversion by cascading. SHB in [49] is built using GaN transistors and it considers wide output voltage range (330-750 V) but the control of the converter is not straightforward.

### C. INTEGRATED OBC and APM TOPOLOGIES

Multiple 800 V OBC topologies integrate the 12 V auxiliary power module (APM) to reduce component count and

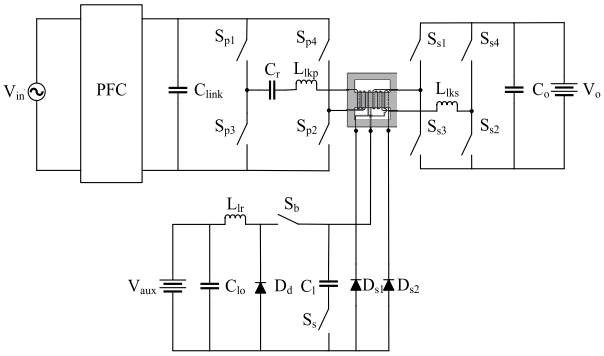


**FIGURE 10.** Combined OBC and APM system [69].

increase power density. Fig. 10 shows the integrated OBC proposed in [69]. This topology aims to improve efficiency compared to a conventional approach with separate converters and reduces component count by reusing switches on the HV battery side and utilizing only one transformer. The topology has two modes: charging and driving. In the charging mode, the grid charges the HV battery through the PFC converter and an LLC converter. The PFC converter regulates the voltage at the DC-link which allows the LLC converter to operate at constant resonant frequency, resulting in high efficiency [70] due to soft switching. In the driving mode, the OBC primary and PFC circuit are inactive and the OBC secondary circuit operates as a PSFB to send power from the high-voltage battery to the low-voltage auxiliary bus. The low-voltage secondary side utilizes a buck converter to charge the 12 V battery. The multiwinding transformer has a unique connection on the low-voltage side in order to reduce inductance compared to the OBC path as in the driving mode, the converter operates as PSFB and the transformer needs to have higher turns ratio and lower leakage inductance. The charging mode has 70% higher leakage inductance than the driving mode. The topology is capable of charging both the auxiliary and high-voltage battery simultaneously due to the inclusion of a decoupling inner buck converter, which has a decoupling capacitor Cl, and in order to separate the converter from charging the auxiliary battery and main battery, switch Ss is switched ON. Therefore, the buck converter can be designed independently using the low voltage side decoupling.

The converter has 21 components, including three inductors, four capacitors, one isolating transformer, ten switches rated at 1200V/20A, and three diodes. The 3.3 kW prototype is built using SiC MOSFETs and achieves a peak efficiency of 97.9%. The transformer volume is 22% less than a conventional separate topology, and this reduces overall volume by 10%, however, the efficiency is 0.2% less than the conventional converter. Furthermore, the control method increases the input current ripple and introduces high THD.

Fig. 11 shows an integrated OBC/APM for 800 V BEVs that focuses on minimizing the number of components while providing a 400 V bus for higher voltage auxiliary loads such as air conditioning [71]. Fig. 11(a) shows the entire topology, which works in two modes: OBC charging and driving. When

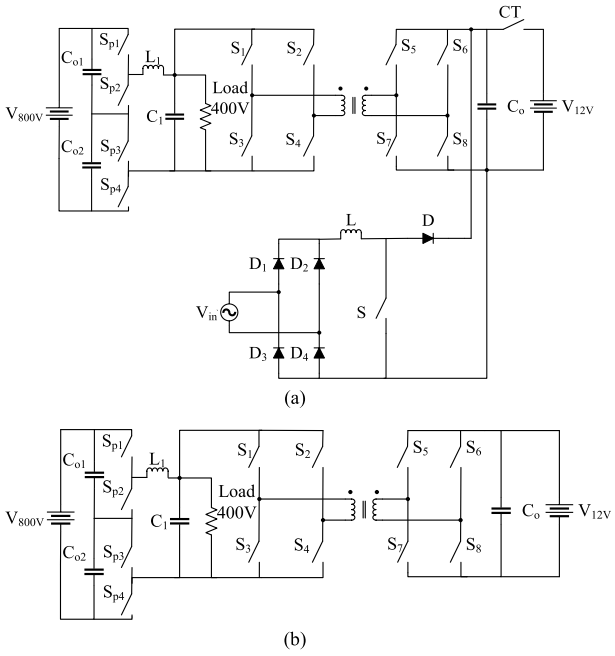


**FIGURE 11.** (a) APM integrated battery charger [71] (b) APM integrated battery charger equivalent circuit in driving mode [71].

the grid is charging the 800 V battery, the contactor CT is open so that the output of the PFC boost converter can be much higher than 12 V. An isolated DAB topology sends the charging power to the 400 V bus, which is then stepped up to 800 V. The DAB operates with soft switching over a wide load range. Fig. 11(b) shows the equivalent circuit in driving mode (when the grid is not connected), and CT has been closed to connect the 12 V battery. A single conventional transformer is used to obtain galvanic isolation between the grid and 800 V battery during charging, as well as between the 800 V battery and the 12 V bus during driving. However, during charging, the AC/DC and PFC converter are connected to the 12 V chassis ground which may pose safety concerns.

The converter has 26 components, including two inductors, four capacitors, one isolating transformer, thirteen switches rated at 650V/21A, and five diodes. The 3.3 kW simulated model is built using SiC MOSFETs and achieves a peak simulated efficiency of 90%. Overall, this topology is flexible due to its extra 400 V connection and uses a single conventional transformer but could benefit from improved efficiency.

Integrated structures are multifunctional and can help increase the power density of the system. Reference [69] uses a single multiwinding transformer to connect the secondaries of both OBC and APM, meaning it can charge the high voltage and low voltage battery at the same time. Reference [71] uses a single conventional transformer for its integrated charger using a DAB-based topology, which allows soft switching over a wide output range.

### D. BIDIRECTIONAL OBCs

Bidirectional OBC topologies can be useful for home or grid support from the vehicle battery. A bidirectional isolated

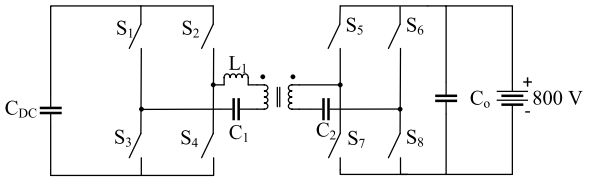


**FIGURE 12.** Resonant DAB-based bidirectional charger [72].

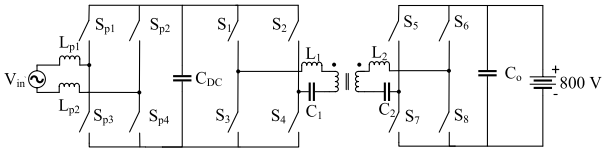


**FIGURE 13.** Full bridge CLLC-based bidirectional charger [73].

DC-DC converter based on the resonant DAB topology is developed in [72] for 800 V onboard charging, and is shown in Fig. 12. This topology has a limited switching frequency range and low turn-off current. Magnetic integrated technology has been used to reduce the transformer size by half. Phase shifted control is used to control the gain of the converter. This converter has 14 components including one inductor, four capacitors, one transformer, and eight switches. The primary switches are 650 V rated GaN switches and the secondary ones are 1200 V rated SiC switches. The experimental prototype is rated at 6.6 kW for charging mode and at 6 kW for discharging mode, and the converter achieves a peak efficiency of 98.3%. The topology is simple, reliable, allows soft switching, and is capable of synchronous rectification, but it has large output ripple current.

Reference [73] proposes a CLLC-based bidirectional isolated 800 V onboard charger with wide output voltage range. Fig. 13 shows the 1-phase version of the converter, though a 3-phase version is also presented in [73]. The converter has the full-bridge configuration and can operate in both buck and boost mode. This topology achieves ZVS with a low magnetizing current which reduces the conduction loss and turn-off switching loss. The efficiency is highest at resonant frequency. This control scheme uses a combination of pulsed frequency modulation and phase shift modulation. The converter has 22 components including four inductors, four capacitors, one transformer, and twelve SiC-based switches rated at 1200 V. A 6.6 kW 1-phase prototype was built which achieved 95% peak efficiency in charging mode and 96% peak efficiency in discharging mode.

### *E. THREE PHASE OBCs*

It may be useful for 800 V BEVs to have the ability to connect to both 1-phase and 3-phase grid connections for Level 2 charging, so that faster charging can be completed when 3-phase connections are available. Thus, this subsection performs a brief review of published 3-phase 800 V OBC topologies, to ensure a comprehensive review in this article.

A single-stage 3-phase high-frequency LLC converter incorporating a multi-resonant boost full bridge topology with PFC operation is proposed in [74]. This topology aims to improve power density and has a peak efficiency of 91.5%. This topology converts 3-phase utility frequency AC to high frequency 1-phase AC without a DC link, which results in a simpler structure with potentially lower cost. The 3-phase line currents are regulated in phase with the 3-phase voltages to attain PFC and the AC inductor currents are controlled in DCM and thus, source voltage detection is not necessary, reducing the additional sensor cost in the system. The parallel circuit configuration at the output, with 120° phase shift between modules, reduces the low and high frequency ripples. Soft switching is accomplished over a varied load power range due to the high frequency transformer magnetizing current in the LLC topology.

The proposed 3-phase OBC from [33] has a soft switching interleaved boost converter after the PFC boost converter, which utilizes an auxiliary resonant circuit. This topology contributes to cost reduction and has a peak efficiency of 98.78%. However, this is a non-isolated design, which may raise safety concerns due to leakage current [75]. The main advantages of this converter are the wide soft switching range, the interleaved structure for current ripple reduction, DCM operation for reducing input side conduction power loss, high efficiency, and a high voltage conversion ratio. However, high voltage rated semiconductors are required.

Reference [76] proposes an interleaved isolated 3-phase OBC with PFC and a wide voltage range capability. This topology aims to enhance efficiency and achieves 95.3% peak efficiency. It has two half bridge voltage-fed isolated PFC circuits in each module, which has a parallel input series output structure operating in DCM interleaved mode. The switches on the primary side have high frequency due to ZVS and ZCS, which enhances efficiency and power density. The leakage inductance of the transformer is utilized as the primary inductor. The control loop is simple with only a single voltage loop as the primary switches have fixed frequency with 50% duty cycle, and feed-forward compensation is used to meet harmonic standards.

A modular single-stage electrolytic capacitor-less 3-phase OBC which can work with 1-phase grids as well is proposed in [77]. This topology aims to reduce control complexity and has a peak efficiency of 97.01%. The topology is based on an interleaved bridgeless totem-pole structure which eliminates the bridge structure and reduces switch count. Soft switching is accomplished from a duty cycle adjustment strategy for low input voltage. The topology is capable of increasing transformer primary voltage owing to its current fed nature. Hence, the primary and secondary voltage difference decreases by regulating the duty cycle in the primary as per the grid and battery voltage variation. As a result, the ZVS turn on of all the switches is maintained over a wide input and output voltage range. This topology uses a simple control strategy using a single control variable of the phase shifted angle. The output current is converted to DC current by controlling the

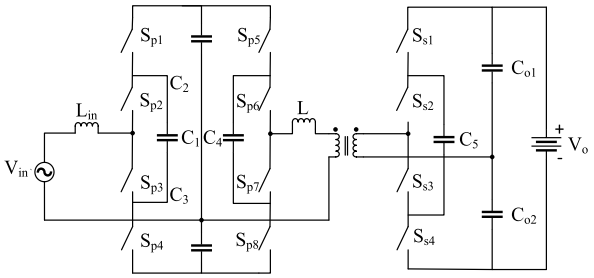


**FIGURE 14.** GaN systems 800 V OBC topology [53].

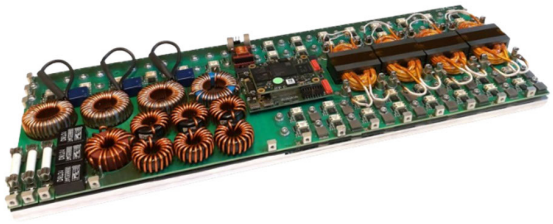

**FIGURE 15.** Infineon technologies 800 V OBC [54].

second harmonic current of the output current to zero using proportional-resonant (PR) control.

The topology proposed in [78] uses three phases that boost the input voltage to 800 V DC. This topology contributes to efficiency and power density improvement, having a peak efficiency of 95.8%. In this converter, each phase has two half bridges and a coupled inductor. It is also capable of bidirectional power transfer for feeding power to the grid. However, its transformer-less design may raise safety concerns due to potential leakage current, though active suppression techniques can be employed [76]. This topology is called active frontend and is popular in industrial applications. It can be controlled using sophisticated vector control strategies.

Three phase chargers can provide higher voltage charging compared to single phase chargers and these do not have the issue of second order harmonics at the output. The LLC-based topology proposed in [74] does not use a DC link, improving the power density and making it cost effective. Reference [33] proposed a non-isolated structure which might have the disadvantage of leakage current, however, this converter attains wide soft switching range and lower current ripple. The topology in [76] accomplishes wide output voltage range and has a simple control scheme for its operation, whereas [77] proposed a topology which is capable of both single and three phase charging. It uses a totem-pole based topology hence, bidirectional charging may be possible. Reference [78] proposed a transformer-less topology with bidirectional charging capabilities, however, it uses complicated vector control for its operation.

Reference [79] proposes a 3-phase topology where the Vienna converter is used for the PFC stage and an LLC resonant converter is used for the isolated DC-DC stage. This topology contributes to power density improvement and has a peak efficiency of 96%. The main advantages of the charger are the soft switching due to the resonant stage, portability, and highly efficient wide output voltage range. However, the reliability of the converter is compromised due to higher number of switches.

### F. INDUSTRIAL 800 V OBCs

GaN Systems announced its 800 V OBC shown in Fig. 14 at APEC 2023, which is rated at 11 kW. By using GaN switches with fast switching transients, a high switching frequency can be used, leading to smaller passive components and high-power density. The OBC has a three-level flying capacitor topology for a bridgeless totem-pole PFC structure for the AC/DC conversion, and a multilevel DAB for the DC/DC conversion. Importantly, this topology allows for the use of 650 V GaN switches in an 800 V OBC. The AC/DC part achieves a peak efficiency of 99% and the DC/DC part achieves a peak efficiency of 98.5% [53], [80]. The resulting power density is 36% higher than a comparable SiC design, and the total converter cost is 15% lower than a comparable SiC design, due to the smaller passive components [80].

Infineon Technologies has developed a next generation GaN-based OBC architecture with a high power density of 10 kW/L, as shown in Fig. 15 [54]. This 3-phase topology rated at 10 kW provides a wide output voltage range of 250-1000 V and handles up to 25 A. It has a Vienna rectifier PFC providing a controlled split DC-link, connected to four DAB converters. The switching frequencies are 560 kHz for the Vienna rectifier and 140-400 kHz for the DAB stage. The topology uses the single-channel functionally isolated EiceDRIVER™ (1EDF5673K), 600 V rated CoolGaN™ GIT HEMT (IGOT60R070D1), and 1200 V rated SiC Schottky CoolSiC™ diodes (IDM10G120C5). GaN GIT HEMTs rated at 600 V are employed in the system for output voltage regulation. DABs are capable of bidirectional and ZVS operation which makes them a good fit for high frequency OBCs.

Innolectric's 800 V OBC 0BC82 [55] provides flexibility for AC and DC charging, and is shown in Fig. 16, though the circuit topology is not publicly available. The OBC achieves high efficiency of over 94% at 22 kW and 96% at 10 kW. It is capable of both 1-phase and 3-phase charging. The maximum input current per phase is 32 A and the output DC current is up to 45 A. The OBC has integrated DC charging functionality, with charging communications for AC and DC. The AC charging function is based on PWM communication, and the DC charging is based on power line communication (PLC).

MTA manufactures 800 V OBC HPC22 under the EDA brand, as shown in Fig. 17 [56], [81], though the circuit topology is not publicly available. The HPC22 is capable of 1-phase (7.3 kW) and 3-phase (22 kW) charging. It has an efficiency of over 94%, high power factor, and low THD. There is galvanic isolation between the vehicle and the grid, DC fast charging communication, DC connector external interlock monitoring, and short circuit and reverse polarity protection at the output.

**FIGURE 16.** OBC82 INNOLECTRIC 800 V OBC [55].

**FIGURE 17.** HPC22 MTA-EDN 800 V OBC [56].

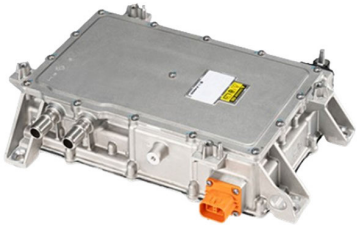

**FIGURE 18.** Magna 800 V charger CU1072 and CU2011 [82].

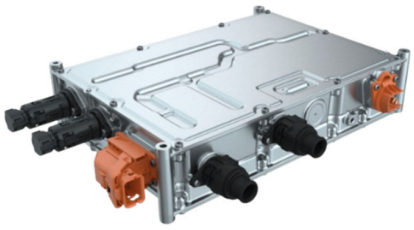

**FIGURE 19.** Valeo 800 V OBC [83].

LG Magna offers an 800 V OBC, as shown in Fig. 18 [82]. Though the circuit topology is not publicly available, features of the OBC include: adaptability to a wide range of AC grid voltages, input filter for noise reduction, PFC for THD improvement and to achieve high efficiency, and integrated magnetic design for high power density. The backend DC/DC converter allows for reliable power transfer to the battery. The OBC efficiency peaks at 95%, and power ratings are available from 3.6 kW to 11 kW.

Valeo has introduced its 4th generation OBC supporting 400-800V at 7/11/22 kW output powers, and is shown in Fig. 19 [83]. It is capable of both 1-phase and 3-phase charging. It achieves an efficiency of 96% and a power density of 2 kW/L. It has several communication features such as CAN, IEC 61851, SAE J1772, GB/T, ISO 15118 PLC, CHAdeMO and can be used on passenger cars and buses. Huawei's 11 kW

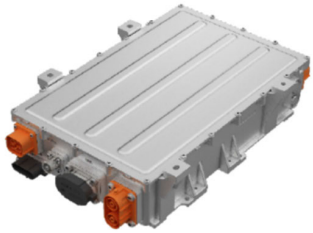

**FIGURE 20.** Huawei 800 V OBC [84].

OBC shown in Fig. 20 [84] has an output voltage range from 400-800V. It has a 1-phase efficiency of 94% and 3-phase efficiency of 94.5%. It uses a liquid cooling heat dissipation system and weighs below 16 kg.

OBCs from industry generally use two-stage structures where LLC, DAB, and PSFB structures are common choices for their backend. However, GaN Systems proposed a flying capacitor-DAB-totem pole topology to allow 800 V charging with the use of 650 V GaN switches [53], and achieves high power density. Infineon Technologies [54] also uses a GaN-based architecture, but with a Vienna-DAB topology, which is capable of soft switching and bidirectional charging. Other common features of industrial products include the ability to charge from 1-phase and 3-phase inputs [55], [56], [82], and the ability to charge both 400 and 800V batteries [83], [84].

## IV. TOPOLOGY COMPARISON

This section provides a comparison of the 800 V 1-phase OBC topologies reviewed in this article. Table 2 categorizes the converters and compares them based on critical design parameters such as the component count, number of transformers, passive components, and semiconductors, switch voltage and current stress, conducting switching devices in a period, mode of operation, sensor count, peak efficiency, and power rating. Most topologies have one transformer for galvanic isolation but [35], [61], and [67] use two transformers. References [34] and [77] have high passive component count at 15 and 16, respectively. Reference [35] uses 16 semiconductor devices to implement its single stage structure. Reference [69] has the highest number of switching devices conducting in one period, which can increase conduction losses. The DCM design has been opted by topologies [2], [34], [35], [61], [71], [77] to reduce the sensor count, thereby making the system robust, reliable, and immune to noise. However, the downside to DCM operation is high ripple current. The peak efficiency for all the topologies is above 95% where [35] reports the highest peak efficiency of 97.9% at 2.4 kW. The GaN Systems 800 V OBC has a component count of 22, using 12 GaN switches which achieves 97.52% efficiency at 11 kW. References [2], [34], [35], [49], [53], [61], and [71] use 650 V rated switches whereas IPOP-DAB [67] and [69] use 1200 V rated switches. Overall, compared to two-stage topologies, single-stage structures offer the potential advantages of higher efficiency and higher power density (due to no requirement for DC link capacitors), yet they also

**TABLE 2. Comparison of different 800 V OBC configurations.**

| Topology | Component Count | Trans-formers | Capac-itors | Induc-tors | Switches/ Diodes | Switching devices in $T_s$ | Mode | Sensors | Peak Efficiency (%) | Rated Power (W) |
|---|---|---|---|---|---|---|---|---|---|---|
| Single-Stage | | | | | | | | | | |
| BL-Interleaved [35] | 27 | 1 | 6 | 4 | 8/8 | 5 | DCM | 1 | 97.9 | 2400 |
| BL-Voltage doubler [34] | 24 | 1 | 11 | 2 | 8/2 | 3 | CCM | 2 | 97 | 5000 |
| Two-Stage | | | | | | | | | | |
| Differential [61] | 17 | 1 | 8 | 2 | 4/2 | 1 | - | - | - | 2000 |
| 400V optimized OBC [2] | 15 | 1 | 1 | 1 | 6/6 | 1 | - | - | 97.1 | 3300 |
| IPOP-DAB [67] | 22 | 2 | 4 | - | 16/0 | - | CCM | 5 | 96.12 | 11500 |
| IPOS-DAB [67] | 22 | 2 | 4 | - | 16/0 | - | CCM | 6 | 96.22 | 11500 |
| ML-DAB [67] | 20 | 1 | 3 | - | 12/4 | - | CCM | 4 | 95.66 | 11500 |
| SHB [49] | 18 | 1 | 7 | 2 | 8/0 | - | - | - | 97 | 6600 |
| Integrated | | | | | | | | | | |
| OBC-APM [69] | 20 | 1 | 5 | 1 | 10/3 | 7 | CCM | 8 | 97.9 | 3300 |
| Aux-integrated [71] | 26 | 1 | 4 | 2 | 13/5 | 1 | - | - | - | - |
| 1,3 – phase [77] | 48 | 3 | 7 | 6 | 30/0 | 3 | DCM | 1 | 97.01 | 11000 |
| Industrial | | | | | | | | | | |
| GaN Systems [53] | 22 | 1 | 7 | 2 | 12/0 | - | - | - | 97.52 | 11000 |

can have higher current ripple. THD and PF are important metrics of 1-phase OBC topologies, but since many research papers test only the DC-DC part of the OBC, they were unable to report these values.

## V. FUTURE TRENDS

### A. WIDE BANDGAP DEVICE USAGE

WBG devices allow operation at higher switching frequencies and temperatures compared to traditional silicon switches. Thus, WBG devices such as GaN and SiC align with the future trends of 800 V OBCs as employing these devices can increase power density (higher switching frequency reduces passive component size), reduce cost (smaller passive components), and increase efficiency [49]. Commercial GaN semiconductors are currently rated from 80V-650V [51], [52], and thus 800 V OBC topologies that eliminate the need for 1200 V rated devices can benefit from GaN technology. To aid in this direction, higher power rated GaN devices would reduce the need for paralleling, and further improvements should be made on reliability issues so that they are more robust for high power application [85]. The voltage rating of GaN devices should be increased to accommodate high voltage battery chargers and some companies have performed research and development in this direction [86]. SiC semiconductors have better gate oxide reliability, are easy to use, and are robust with excellent voltage blocking capabilities [87]. SiC offers superior performance in high voltage and high temperature applications. GaN is superior in power density improvement, but the gate driver design for GaN switches can be complicated. Deploying these WBG devices would demand proper redesign of gate driver boards to make it compatible with the device specification for better performance of the device. GaN Systems has recently introduced an 800 V OBC topology rated at 11 kW using GaN devices, which has power density higher by 36% and total cost lower by 15%, in comparison to a design based on SiC devices [53], [80].

### B. COMPACT TOPOLOGIES

The most popular topologies for OBCs are the two-stage ones with a DC link [47], [61], which has a frontend AC/DC PFC part and a backend isolated DC/DC part [33], [34]. Recent research is moving towards single-stage topologies [34], [35], [36], [88] as the DC link capacitor is a heavy component which adds to the weight of the system and affects the power density. The power density and weight are important aspects for OBC design since packaging components within the physical vehicle constraints is always challenging, and extra weight reduces total vehicle efficiency. The capacitor removal can also enhance the reliability of the system, as capacitors can fail and their capacitance degrades over time. The novel single-stage topologies aim to reduce switch count as well as component count in general to improve the power density and reliability of the OBC [53], [71]. Reducing the switch count can increase reliability, as these are the components which fail most often in the system and can decrease the OBC cost. Reduction of passive components can improve power density as well.

### C. FLEXIBLE CHARGING

Most OBC designs focus on grid-to-vehicle (G2V) charging, but it can be beneficial to have flexible charging options such as vehicle-to-grid (V2G), vehicle-to-home (V2H), and vehicle-to-vehicle (V2V) [89], [90]. Flexible charging technology such as V2G allows BEV charging at lower cost at night and the power can be sold back to the grid at higher cost during the daytime, resulting in profit [91]. V2G is a flexible charging option which helps to maintain reliability of the grid and allows financial benefits to the BEV owner. This technology can allow real time communication among the charging station, the car, the EV driver, and the home to enable a charging process control, and offers energy usage insights for optimizing and personalizing charging sessions. The user can view and control charging sessions from their phones directly [18].

The V2G charging feature is an important facet of smart grids that intelligently control and balance loads, such as EV chargers, homes, etc. Within a smart grid, sensors and communication networks monitor loads to ensure grid overloading does not occur, often using cloud connected systems. With V2G charging capability in the smart grid, the grid controls can also decide when it is beneficial to discharge the vehicle battery to power the grid, generally at times of heavy load or when frequency regulation problems. The flexibility of the smart grid can also lead to higher penetrations of variable renewable energy sources such as solar and wind power, and EV batteries connected to the grid with V2G technology can provide useful temporary energy storage for these variable energy sources. Since 800 V BEVs may help increase BEV adoption due to faster charging times, equipping these vehicles with V2G technology could also help accelerate the path to a smart and sustainable grid.

The V2H technology uses the BEV battery as a backup power source for the home in times of emergency such as grid power outages. V2H technology can be used to power appliances using the BEV battery (typical to a 120 V system) [92]. Also, V2V charging can help combat range anxiety because it allows the sharing of energy from one BEV to another [93], [94], making the BEV into a portable power source. However, for these bidirectional OBC topologies, the cost and the control complexity will increase. Although there are several articles on 400 V bidirectional charging topologies [89], [95], there are fewer for 800 V bidirectional topologies [72], [73]. GM is already testing V2G and V2H technologies [96], [97].

## VI. CONCLUSION

This article presents a detailed topological review of state-of-the-art 800 V OBCs for passenger BEVs and discusses the challenges in shifting from 400 V to 800 V OBCs. Single-stage, two-stage, integrated, 3-phase, and bidirectional topologies are discussed, and efficiencies as well as component counts are considered. In the main comparison of 1-phase 800 V OBCs, it is found that the single-stage structures can have a more compact design due to not having DC-link capacitors, and can achieve high peak efficiencies, though the control can be more complex. The topology proposed by GaN Systems is a promising single-phase single-stage topology with a component count of 22 and a peak efficiency of 97.52%. Though the proposed single-stage structures provide compact solutions, the component reduction and compactness may be further improved. Most two-stage structures use LLC- and DAB- based topologies. The DAB-based topologies may be further improved by incorporating the bidirectional charging feature. The integrated topologies discussed in the article use a single transformer solution to also connect to the low-voltage bus, increasing overall power density. This article also reviews industrial products where most of the chargers are capable of both single- and three-phase charging, and some can charge both 400 and 800 V batteries. Future trends are discussed, including the use of wide bandgap devices, compact design, and flexible charging technologies.

## REFERENCES

[1] L. Dickerman and J. Harrison, "A new car, a new grid," *IEEE Power Energy Mag.*, vol. 8, no. 2, pp. 55–61, Mar. 2010.
[2] J.-Y. Kim, B.-S. Lee, D.-H. Kwon, D.-W. Lee, and J.-K. Kim, "Low voltage charging technique for electric vehicles with 800 V battery," *IEEE Trans. Ind. Electron.*, vol. 69, no. 8, pp. 7890–7896, Aug. 2022.
[3] C. C. Chan, "The state of the art of electric, hybrid, and fuel cell vehicles," *Proc. IEEE*, vol. 95, no. 4, pp. 704–718, Apr. 2007.
[4] (2023). *Global Electric Car Sales Rose 31% in 2023—Rho Motion | Reuters*. Accessed: Feb. 12, 2024. [Online]. Available: https://www.reuters.com/business/autos-transportation/global-electric-car-sales-rose-31-2023-rho-motion-2024-01-11/
[5] E. Latulippe and K. Mo. (2019). *Outlook for Electric Vehicles and Implications for the Oil Market*. [Online]. Available: https://www.bankofcanada.ca/wp-content/uploads/2019/06/san2019-19.pdf
[6] G. H. Broadbent, G. Metternicht, and D. Drozdzewski, "An analysis of consumer incentives in support of electric vehicle uptake: An Australian case study," *World Electr. Vehicle J.*, vol. 10, no. 1, p. 11, Mar. 2019.
[7] J. Voelcker. (2016). *Porsches 800-Volt Fast Charging for Electric Cars: Why It Matters*. [Online]. Available: https://www.greencarreports.com/news/1106954_porsches-800-volt-fast-charging-for-electric-cars-why-it-matters
[8] N. Deb and R. Singh, "An 800V end to end SiC powertrain to accommodate extremely fast charging," *J. Energy Power Technol.*, vol. 5, no. 1, p. 007, 2023, doi: 10.21926/jept.2301007.
[9] V. Reber. (2016). *E-Power: New Possibilities With 800-Volt Charging*. [Online]. Available: https://www.porscheengineering.com/peg/en/about/magazine/
[10] *Porsche Charging All-electric Porsche Models Quickly and Easily—Porsche USA*. Accessed: Aug. 1, 2024. [Online]. Available: https://www.porsche.com/usa/
[11] *Aston Martin to Display Rapide E At Fully Charged Live*. Accessed: Aug. 1, 2024. [Online]. Available: https://insideevs.com/news/353275/aston-Martin-rapide-e-fully-charged-live/
[12] *Hyundai IONIQ 5 Charging Time, Range, and Cost | EVBox*. Accessed: Aug. 1, 2024. [Online]. Available: https://evbox.com/uk-en/electric-cars/hyundai/
[13] *Genesis G80 Electrified Luxury*. Accessed: May 16, 2023. [Online]. Available: https://ev-database.org/car/1703/Genesis-G80-Electrified-Luxury
[14] *Audi E-Tron GT RS*. Accessed: Aug. 1, 2024. [Online]. Available: https://ev-database.org/car/1153/Audi-e-tron-GT-RS
[15] (2022). *Kia EV6 U.S. Specs Compared: Battery, Range, Price And More*. [Online]. Available: https://insideevs.com/news/565543/kia-ev6-comparison-battery-range/
[16] (2020). *High Power Charging; Fast Charging Just Got Faster*. [Online]. Available: https://new.abb.com/evcharging/
[17] M. H. Mobarak and J. Bauman, "Vehicle-directed smart charging strategies to mitigate the effect of long-range EV charging on distribution transformer aging," *IEEE Trans. Transport. Electrific.*, vol. 5, no. 4, pp. 1097–1111, Dec. 2019.
[18] X. Huang, J. Meng, W. Liu, F. Ru, C. Duan, X. Xu, D.-I. Stroe, and R. Teodorescu, "Lithium-ion battery lifetime extension with positive pulsed current charging," *IEEE Trans. Ind. Electron.*, vol. 71, no. 1, pp. 1–8, Jan. 2023.
[19] D. Clark. (2009). *Real-Time '$CO_2$ Intensity' Site Makes the Case for Midnight Dishwashing*. Accessed: Nov. 6, 2023. [Online]. Available: https://www.theguardian.com/environment/2009/jul/17/realtime-carbon-counter
[20] *North American Voltage Ranges*. Accessed: Aug. 1, 2024. [Online]. Available: https://quick220.com/pages/north-american-voltage-ranges
[21] J. Locke. (2023). *Single Phase vs. Three Phase Power: North American Edition*. Accessed: Nov. 6, 2023. [Online]. Available: https://blog.bartellglobal.com/single-phase-vs-three-phase-power-north-american-edition
[22] (2021). *Single and 3-Phase Charging—The Difference*. Accessed: Nov. 6, 2023. [Online]. Available: https://www.50five.com/en-gb/e-mobility/blog/single-and-3-phase-charging
[23] (2023). *Higher Voltage Packs*. Accessed: Nov. 6, 2023. [Online]. Available: https://www.batterydesign.net/higher-voltage-packs/

[24] C. Jung, "Power up with 800-V systems: The benefits of upgrading voltage power for battery-electric passenger vehicles," *IEEE Electrific. Mag.*, vol. 5, no. 1, pp. 53–58, Mar. 2017.

[25] I. Aghabali, J. Bauman, P. J. Kollmeyer, Y. Wang, B. Bilgin, and A. Emadi, "800-V electric vehicle powertrains: Review and analysis of benefits, challenges, and future trends," *IEEE Trans. Transport. Electrific.*, vol. 7, no. 3, pp. 927–948, Sep. 2021.

[26] R. Pradhan, N. Keshmiri, and A. Emadi, "On-board chargers for high-voltage electric vehicle powertrains: Future trends and challenges," *IEEE Open J. Power Electron.*, vol. 4, no. 1, pp. 189–207, Aug. 2023.

[27] S. Haghbin, S. Lundmark, M. Alakula, and O. Carlson, "Grid-connected integrated battery chargers in vehicle applications: Review and new solution," *IEEE Trans. Ind. Electron.*, vol. 60, no. 2, pp. 459–473, Feb. 2013.

[28] B. Singh, B. N. Singh, A. Chandra, K. Al-Haddad, A. Pandey, D. P. Kothari, "A review of single-phase improved power quality AC–DC converters," *IEEE Trans. Ind. Electron.*, vol. 50, no. 5, pp. 962–981, Jul. 2003.

[29] B. Singh, B. N. Singh, A. Chandra, K. Al-Haddad, A. Pandey, and D. P. Kothari, "A review of three-phase improved power quality AC–DC converters," *IEEE Trans. Ind. Electron.*, vol. 51, no. 3, pp. 641–660, Jun. 2004.

[30] J. Xiaoping, "A new AC charging system with orderly charging for electric vehicles," in *Proc. 5th Int. Conf. Power Electron. Syst. Appl.*, Dec. 2013, pp. 1–4.

[31] A. R. Bhatti, Z. Salam, M. J. B. A. Aziz, and K. P. Yee, "A critical review of electric vehicle charging using solar photovoltaic," *Int. J. Energy Res.*, vol. 40, no. 4, pp. 439–461, Mar. 2016.

[32] P. Paulraj. *Charging Basics 102: Electric Vehicle Charging Levels, Modes and Types Explained: North America Vs. Europe Charging Cables and Plug Types*. Accessed: Jul. 21, 2021. [Online]. Available: https://www.emobilitysimplified.com/2019/10/evcharging-levels-modes-types-explained.html

[33] N. A. Ahmed, B. N. Alajmi, I. Abdelsalam, and M. I. Marei, "Soft switching multiphase interleaved boost converter with high voltage gain for EV applications," *IEEE Access*, vol. 10, pp. 27698–27716, 2022.

[34] M. Abbasi and J. Lam, "An SiC-based AC/DC CCM bridgeless onboard EV charger with coupled active voltage doubler rectifiers for 800-V battery systems," in *Proc. IEEE Appl. Power Electron. Conf. Expo. (APEC)*, USA, Mar. 2020, pp. 905–910.

[35] M. Abbasi, K. Kanathipan, and J. Lam, "An interleaved bridgeless single-stage AC/DC converter with stacked switches configurations and soft-switching operation for high-voltage EV battery systems," *IEEE Trans. Ind. Appl.*, vol. 58, no. 5, pp. 5533–5545, Sep. 2022.

[36] S. Dutta, S. Gangavarapu, A. K. Rathore, R. K. Singh, S. K. Mishra, and V. Khadkikar, "Novel single-phase cuk-derived bridgeless PFC converter for on-board EV charger with reduced number of components," *IEEE Trans. Ind. Appl.*, vol. 58, no. 3, pp. 3999–4010, May 2022.

[37] Y. Zhang, G. Yang, X. He, M. Elshaer, W. Perdikakis, H. Li, C. Yao, J. Wang, K. Zou, Z. Xu, and C. Chen, "Leakage current issue of non-isolated integrated chargers for electric vehicles," in *Proc. IEEE Energy Convers. Congr. Expo. (ECCE)*, Sep. 2018, pp. 1221–1227.

[38] J.-Y. Lee, Y.-S. Jeong, and B.-M. Han, "An isolated DC/DC converter using high-frequency unregulated *LLC* resonant converter for fuel cell applications," *IEEE Trans. Ind. Electron.*, vol. 58, no. 7, pp. 2926–2934, Jul. 2011.

[39] (2024). *Design Guide*. Accessed: Apr. 19, 2024. [Online]. Available: https://www.transphormusa.com/en/document/design-guide-200-khz-phase-shift-full-bridge-for-3-3kw-electric-vehicle-on-board-charger/

[40] D. S. Gautam, F. Musavi, M. Edington, W. Eberle, and W. G. Dunford, "An automotive onboard 3.3-kW battery charger for PHEV application," *IEEE Trans. Veh. Technol.*, vol. 61, no. 8, pp. 3466–3474, Oct. 2012.

[41] F. Musavi, M. Craciun, D. S. Gautam, W. Eberle, and W. G. Dunford, "An LLC resonant DC–DC converter for wide output voltage range battery charging applications," *IEEE Trans. Power Electron.*, vol. 28, no. 12, pp. 5437–5445, Dec. 2013.

[42] *IEEE Standard for Interconnection and Interoperability of Distributed Energy Resources With Associated Electric Power Systems Interfaces*, Standard IEEE Std 1547-2018, 2018, pp. 1–138.

[43] *Power Quality Requirements for Plug-In Electric Vehicle Chargers—Part 1: Requirements*, Standard SAE J2894-1, 2019.

[44] *Electromagnetic Compatibility (EMC)—Part 3–2: Limits—Limits for Harmonic Current Emissions*, Standard IEC 61000-3-2, 2018.

[45] M. A. Hannan, Md. M. Hoque, A. Hussain, Y. Yusof, and P. J. Ker, "State-of-the-Art and energy management system of lithium-ion batteries in electric vehicle applications: Issues and recommendations," *IEEE Access*, vol. 6, pp. 19362–19378, 2018.

[46] Q.-Q. Yu, R. Xiong, L.-Y. Wang, and C. Lin, "A comparative study on open circuit voltage models for lithium-ion batteries," *Chin. J. Mech. Eng.*, vol. 31, no. 1, pp. 1–65, Dec. 2018.

[47] D. Cesiel and C. Zhu, "A closer look at the on-board charger: The development of the second-generation module for the Chevrolet volt," *IEEE Electrific. Mag.*, vol. 5, no. 1, pp. 36–42, Mar. 2017.

[48] F. Jin, A. Nabih, C. Chen, X. Chen, Q. Li, and F. C. Lee, "A high efficiency high density DC/DC converter for battery charger applications," in *Proc. IEEE Appl. Power Electron. Conf. Expo. (APEC)*, Jun. 2021, pp. 1767–1774.

[49] S. Mukherjee, J. M. Ruiz, and P. Barbosa, "A high power density wide range DC–DC converter for universal electric vehicle charging," *IEEE Trans. Power Electron.*, vol. 38, no. 2, pp. 1998–2012, Feb. 2023.

[50] X. Huang, Z. Liu, Q. Li, and F. C. Lee, "Evaluation and application of 600 V GaN HEMT in cascode structure," *IEEE Trans. Power Electron.*, vol. 29, no. 5, pp. 2453–2461, May 2014.

[51] Wolfspeed. (2022). *CREE SiC MOSFET Gen2 40mOhm Datasheet*. [Online]. Available: https://assets.wolfspeed.com/uploads/2020/12/

[52] H. Amano et al., "The 2018 GaN power electronics roadmap," *J. Phys. D, Appl. Phys.*, vol. 51, no. 16, Mar. 2018, Art. no. 163001, doi: 10.1088/1361-6463/aaaf9d.

[53] (2023). *GaN Systems 800V 11kW OBC Reference Design—Key Insights*. Accessed: Jul. 31, 2023. [Online]. Available: https://gansystems.com/newsroom/gan-systems-800v-11kw-obc-reference-design/

[54] M. J. Kasper, J. A. Anderson, G. Deboy, Y. Li, M. Haider, and J. W. Kolar, "Next generation GaN-based architectures: From 240W USB-C adapters to 11kW EV on-board chargers with ultra-high power density and wide output voltage range," in *Proc. Int. Exhibition Conf. Power Electron., Intell. Motion, Renew. Energy Energy Manage.*, May 2022, pp. 1–10.

[55] *On-board Charger*. Accessed: Aug. 1, 2024. [Online]. Available: https://innolectric.ag/on-board-charger-2-2/?lang=en

[56] (2024). *Power Electronics*. Accessed: Feb. 14, 2024. [Online]. Available: https://www.mta.it/en/power-electronics

[57] (2016). *Transformer Losses*. [Online]. Available: http://large.stanford.edu/courses/2016/ph240/swafford1/

[58] (2022). *Putting Energy Efficient Transformr Procurement Into Practice: A Guide to Using Total Cost of Ownership When Purchasing Distribution Transformers*. [Online]. Available: https://united4efficiency.org/wp-content/

[59] F. Musavi, W. Eberle, and W. G. Dunford, "A high-performance single-phase bridgeless interleaved PFC converter for plug-in hybrid electric vehicle battery chargers," *IEEE Trans. Ind. Appl.*, vol. 47, no. 4, pp. 1833–1843, Jul. 2011.

[60] C. Olalla, C. Deline, D. Clement, Y. Levron, M. Rodriguez, and D. Maksimovic, "Performance of power-limited differential power processing architectures in mismatched PV systems," *IEEE Trans. Power Electron.*, vol. 30, no. 2, pp. 618–631, Feb. 2015.

[61] H. Sarnago, Ó. Lucía, R. Jiménez, and P. Gaona, "Differential-power-processing on-board-charger for 400/800-V battery architectures using 650-V super junction MOSFETs," in *Proc. IEEE Appl. Power Electron. Conf. Expo. (APEC)*, Jun. 2021, pp. 564–568.

[62] P. S. Shenoy, K. A. Kim, B. B. Johnson, and P. T. Krein, "Differential power processing for increased energy production and reliability of photovoltaic systems," *IEEE Trans. Power Electron.*, vol. 28, no. 6, pp. 2968–2979, Jun. 2013.

[63] P. S. Shenoy and P. T. Krein, "Differential power processing for DC systems," *IEEE Trans. Power Electron.*, vol. 28, no. 4, pp. 1795–1806, Apr. 2013.

[64] B. Zhao, Q. Song, W. Liu, and Y. Sun, "Overview of dual-active-bridge isolated bidirectional DC–DC converter for high-frequency-link power-conversion system," *IEEE Trans. Power Electron.*, vol. 29, no. 8, pp. 4091–4106, Aug. 2014.

[65] F. Krismer and J. W. Kolar, "Efficiency-optimized high-current dual active bridge converter for automotive applications," *IEEE Trans. Ind. Electron.*, vol. 59, no. 7, pp. 2745–2760, Jul. 2012.

[66] R. G. Kheraluwala, D. Gascoigne, D. Divan, and E. Baumann, "Performance characterization of a high-power dual active bridge DC–DC," *IEEE Trans. Ind. Appl.*, vol. 28, no. 6, pp. 1294–1301, Sep. 1992.

[67] R. Pradhan, M. Narimani, and A. Emadi, "Converter topology comparison for a two-stage Level-2 onboard charger in 800-V EV powertrains," in *Proc. 48th Annu. Conf. IEEE Ind. Electron. Soc.*, Oct. 2022, pp. 1–6.
[68] M. Moonem, C. Pechacek, R. Hernandez, and H. Krishnaswami, "Analysis of a multilevel dual active bridge (ML-DAB) DC–DC converter using symmetric modulation," *Electronics*, vol. 4, no. 2, pp. 239–260, Apr. 2015.
[69] D.-W. Lee, B.-S. Lee, J.-H. Ahn, J.-Y. Kim, and J.-K. Kim, "New combined OBC and LDC system for electric vehicles with 800 V battery," *IEEE Trans. Ind. Electron.*, vol. 69, no. 10, pp. 9938–9951, Oct. 2022.
[70] S. Bolte, A. Speerschneider, N. Frehleke, and J. Bucker, "A comparison of on-board chargers for electric vehicles with variable DC-link voltage," in *Proc. IEEE Int. Conf. Smart Energy Grid Eng., Aug.*, Nov. 2015, pp. 1–5.
[71] I. Aghabali, J. Bauman, and A. Emadi, "Analysis of auxiliary power unit and charging for an 800 V electric vehicle," in *Proc. IEEE Transp. Electrific. Conf. Expo. (ITEC)*, Jun. 2019, pp. 1–6.
[72] M. Jia, H. Sun, J. Cai, H. Zhang, Z. Zhou, and J. Chen, "GaN and SiC based 500 kHz resonant bidirectional DC/DC design for 800 V OBCM application," in *Proc. IEEE Appl. Power Electron. Conf. Exposit. (APEC)*, Long Beach, CA, USA, Feb. 2024, pp. 2425–2432.
[73] C. Wei, H. Xie, Y. Liu, Z. Hu, and J. Shao, "A SiC based high efficiency 22kW bi-directional EV on-board charger," in *Proc. Int. Exhibition Conf. Power Electron., Intell. Motion, Renew. Energy Energy Manage.*, May 2021, pp. 1–7.
[74] T. Mishima and S. Mitsui, "A single-stage high-frequency-link modular three-phase *LLC* AC–DC converter," *IEEE Trans. Power Electron.*, vol. 37, no. 3, pp. 3205–3218, Mar. 2022.
[75] A. Dong, D. Sadeghpour, and J. Bauman, "High efficiency GaN-based non-isolated electric vehicle on-board charger with active filtering," in *Proc. IEEE Transp. Electrific. Conf. Expo. (ITEC)*, Jun. 2022, pp. 1307–1313.
[76] S.-W. Choi, S.-T. Oh, M.-W. Kim, I.-O. Lee, and J.-Y. Lee, "Interleaved isolated single-phase PFC converter module for three-phase EV charger," *IEEE Trans. Veh. Technol.*, vol. 69, no. 5, pp. 4957–4967, May 2020.
[77] H. Kim, J. Park, S. Kim, R. M. Hakim, H. P. Kieu, and S. Choi, "Single-stage EV on-board charger with single- and three-phase grid compatibility," in *Proc. IEEE Appl. Power Electron. Conf. Expo. (APEC)*, Jun. 2021, pp. 583–589.
[78] N. Langmaack, G. Tareilus, G. Bremer, and M. Henke, "Transformerless onboard charger for electric vehicles with 800 V power system," in *Proc. IEEE 13th Int. Conf. Power Electron. Drive Syst. (PEDS)*, Toulouse, France, Jul. 2019, pp. 1–5.
[79] S. Ditze, S. Ehrlich, N. Weitz, M. Sauer, F. Aßmus, A. Sacher, C. Joffe, C. Seßler, and P. Meißner, "A high-efficiency high-power-density SiC-based portable charger for electric vehicles," *Electronics*, vol. 11, no. 12, p. 1818, Jun. 2022.
[80] (2023). *GaN Systems Unveils Revolutionary New GaN-Based 800V On-Board Charger (OBC) Reference Design*. [Online]. Available: https://gansystems.com/newsroom/gan-based-800v-on-board-charger/
[81] (2024). *On-Board Chargers—Catalogue*. Accessed: Feb. 16, 2024. [Online]. Available: https://www.mta.it/en/catalogue-on-board-chargers
[82] *On-Board Charger—LG Magna E-Powertrain*. Accessed: Jul. 31, 2023. [Online]. Available: https://lgmagna.com/products/power-electronics/on-board-charger/
[83] (2024). *EV High Voltage On-Board Charger*. Accessed: Apr. 19, 2024. [Online]. Available: https://www.valeo.com/en/catalogue/pts/ev-high-voltage-on-board-charger/
[84] (2024). *11kW 3-in-1 On Board Charging System(High-Voltage) | Huawei Digital Power*. Accessed: Apr. 19, 2024. [Online]. Available: https://digitalpower.huawei.com/en/DriveONE/product_level/on_board_charging_system/detail/45.html
[85] J. Wuerfl, E. Bahat-Treidel, F. Brunner, E. Cho, O. Hilt, P. Ivo, A. Knauer, P. Kurpas, R. Lossy, M. Schulz, S. Singwald, M. Weyers, and R. Zhytnytska, "Reliability issues of GaN based high voltage power devices," *Microelectron. Rel.*, vol. 51, nos. 9–11, pp. 1710–1716, Sep. 2011.
[86] *Transphorm GaN Power FET Portfolio*. Accessed: Aug. 1, 2024. [Online]. Available: https://www.transphormusa.com/en/products/
[87] T. J. C. Sousa, L. Machado, D. Pedrosa, C. Martins, V. Monteiro, and J. L. Afonso, "Comparative analysis of vehicle-to-vehicle (V2V) power transfer configurations without additional power converters," in *Proc. IEEE 14th Int. Conf. Compat., Power Electron. Power Eng.*, vol. 1, Jul. 2020, pp. 88–93.
[88] T. J. C. Sousa, V. Monteiro, J. C. A. Fernandes, C. Couto, A. A. N. Meléndez, and J. L. Afonso, "New perspectives for vehicle-to-vehicle (V2V) power transfer," in *Proc. IECON - 44th Annu. Conf. IEEE Ind. Electron. Soc.*, Washington, DC, USA, Oct. 2018, pp. 5183–5188, doi: 10.1109/IECON.2018.8591209.
[89] M. Kwon and S. Choi, "An electrolytic capacitorless bidirectional EV charger for V2G and V2H applications," *IEEE Trans. Power Electron.*, vol. 32, no. 9, pp. 6792–6799, Sep. 2017.
[90] H. Heydari-doostabad and T. O'Donnell, "A wide-range high-voltage-gain bidirectional DC–DC converter for V2G and G2 V hybrid EV charger," *IEEE Trans. Ind. Electron.*, vol. 69, no. 5, pp. 4718–4729, May 2022.
[91] (2024). *The Many Benefits of V2G Charging*. Accessed: Feb. 14, 2024. [Online]. Available: https://www.evconnect.com/blog/how-a-v2g-charger-can-earn-you-money
[92] (2023). *What Is Bidirectional Charging?*. Accessed: Jul. 31, 2023. [Online]. Available: https://www.evconnect.com/blog/what-is-bidirectional-charging
[93] S. Dutta, A. K. Rathore, and V. Khadkikar, "Single-phase bridgeless converter for on-board EV charger with flexible charging capabilities," *IEEE J. Emerg. Sel. Topics Ind. Electron.*, vol. 4, no. 4, pp. 1–11, Sep. 2023.
[94] S. Dutta, A. K. Rathore, V. Khadkikar, and H. Zeineldin, "Single-phase bridgeless cuk-derived DC–DC converter for vehicle-to-vehicle charge transfer," in *Proc. IEEE Transp. Electrific. Conf.*, Dec. 2021, pp. 1–6.
[95] H. Heydari-doostabad and T. O'Donnell, "A wide-range high-voltage-gain bidirectional DC–DC converter for V2G and G2V hybrid EV charger," *IEEE Trans. Ind. Electron.*, vol. 69, no. 5, pp. 4718–4729, May 2022.
[96] J. M. Gitlin. (2023). *General Motors Will Add Bidirectional Charging To Its Ultium-based EVs*. [Online]. Available: https://arstechnica.com/cars/2023/08/general-motors-will-add-bidirectional-charging-to-its-ultium-based-evs/
[97] (2023). *Site Maintenance*. Accessed: Nov. 06, 2023. [Online]. Available: https://news.gm.com/newsroom.detail.html/Pages/news/us/en/2023/aug/0808-v2h.html

**SUKANYA DUTTA** (Member, IEEE) received the B.Tech. degree in electrical engineering from the Kalinga Institute of Industrial Technology (KIIT), Bhubaneswar, India, in 2019, and the M.A.Sc. degree in electrical and computer engineering from Concordia University, Montreal, Canada, in 2021. She is currently pursuing the Ph.D. degree in electrical engineering with McMaster University, Hamilton, Canada. Her research interests include ac–dc converters, dc–dc converters, controller design, and OBC design for electrified vehicles. She was a recipient of the Concordia Split Merit Scholarship.

**JENNIFER BAUMAN** (Senior Member, IEEE) received the B.Sc. and Ph.D. degrees in electrical engineering from the University of Waterloo, Waterloo, Canada, in 2004 and 2008, respectively. From 2009 to 2016, she was the Director of Research with CrossChasm Technologies, Waterloo, where she led the modeling team on a wide variety of automotive projects. She is currently an Associate Professor of electrical engineering with McMaster University, Hamilton, Canada. Her research interests include power electronic converters for electrified powertrains, vehicle design, modeling, and control, and EV interactions with the smart grids. She is an Associate Editor of IEEE Open Journal of Power Electronics. She is a registered Professional Engineer.